Borrás García, EM.; Tortajada Genaro, LA. (2012). Secondary organic aerosol formation from the photo-oxidation of benzene. Atmospheric Environment. 47:154-163. doi:10.1016/j.atmosenv.2011.11.020.

Secondary organic aerosol formation from the photo-oxidation of benzene

E. Borrás[(a)*], L.A Tortajada-Genaro [(b)]

(a) Instituto Universitario Centro de Estudios Ambientales del Mediterráneo (CEAM-UMH)

(b) Instituto de Reconocimiento Molecular y Desarrollo Tecnológico-Departamento Química, Universitat Politècnica de València

* Author for correspondence:

Esther Borrás García

EUPHORE Department. CEAM-UMH

C/Charles R. Darwin, 14. 46980 Paterna- Valencia – Spain

esther@ceam.es

Phone: +34 96 131 82 27

Fax: +34 96 131 81 90

ABSTRACT

The production of condensate compounds from the degradation of benzene by OH radical chemistry was studied. Secondary organic aerosol (SOA) formation was investigated in the EUPHORE (*European Photoreactor*) simulation chambers. Experiments were performed under different OH-production conditions – addition of H_2O_2, NO or HONO -, in a high-volume reactor, with natural light and in the absence of seed aerosols. The consumption of precursor/reagents, the formation of gas-phase and particulate-phase products and the temporal evolution of aerosol were monitored. Several aerosol physical properties - mass concentration, overall aerosol yield, particle size distribution and density - were determined and found to be clearly dependent on OH radical production and NO_x concentrations. Furthermore, the use of one and/or two products gas-particle partitioning absorption models allowed us to determine the aerosol yield curves. The SOA yield ranged from 1.6 to 9.7 %, with higher SOA formation under low-NO_x conditions. Chemical characterization of the SOA was carried out, determining multi-oxygenated condensed organic compounds by a method based on the gas chromatography-mass spectrometry technique. Several ring-retaining and ring-cleavage products were identified and quantified. The compounds with the highest percentage contribution to the total aerosol mass were 4-nitrobenzene-1,2-diol, butenedioic acid, succinic acid and trans-trans-muconic. In addition, a multigenerational study was performed comparing with the photo-oxidations of phenol and catechol. The results showed that although the mass concentration of SOA produced was different, the physical and chemical properties were quite similar. Finally, we suggest a general mechanism to describe how changes in benzene degradation pathways – rate of OH generation and concentration of NO_x - could justify the variation in SOA production and properties.

Keywords: Benzene, phenol, catechol, SOA yield, multi-oxygenated compounds.

1. INTRODUCTION

Benzene is a major aromatic hydrocarbon air pollutant with an emission rate of 11 Tg year^{-1}, and it plays a critical role in atmospheric chemistry. Atmospheric studies on benzene acquired greater relevance when this volatile organic compound (VOC) became established as a petrol additive, thus increasing its direct emission. Other benzene sources are the chemical industry, biomass burning, cracking of aromatic hydrocarbons, solvent usage and industries related to vegetable oil processing. The increasing levels of this pollutant – up to 5 μg m^{-3} higher than European Directive 2000/69/EC stipulates - are of great concern not only because benzene can promote carcinogenic effects and lung disease in humans but also because it is an important precursor of ground-level ozone (Martin-Reviejo and Wirtz, 2005).

The atmospheric transformations of VOCs, including aromatic hydrocarbons**,** have been widely examined using simulation photoreactors which reproduce reactions isolated from meteorological variations or dispersion (Volkamer et al., 2002). Degradation reactions include photolysis, photo-oxidations and ozonolysis. In the case of benzene, its photo-oxidation is dominated by OH radicals (k_{OH} = 1.22×10^{-12} cm^3 molecule^{-1} s^{-1}), in comparison with its reactions with ozone (k_{O3} = 1. 72×10^{-22} cm^3 molecule^{-1} s^{-1}), NO_3 radicals (k_{NO3} = 1.10×10^{-17} cm^3 molecule^{-1} s^{-1}), other atmospheric radicals or photolysis (Finlayson-Pitts and Pitts, 2000). Thus, the atmospheric degradation is mainly initiated by adding the OH radical to the aromatic ring to form the OH-adduct, which in the presence of O_2 forms phenol and is also in equilibrium with the corresponding peroxy radical (Raoult et al., 2004). Further oxidation channels are influenced by the NO_x concentrations, which modify the reaction rates and the product yields (Berndt and Böge, 2006; Volkamer et al., 2002; Klotz et al., 2002; Raoult et al., 2004).

Nevertheless, there is considerable uncertainty regarding its degradation pathways (Klotz et al., 2002; Berndt and Böge, 2001, 2006). Benzene seems to behave differently from other aromatic hydrocarbons (Kroll and Seinfeld, 2008). This finding is especially significant in terms of the basic underlying formation mechanism of secondary organic aerosol (SOA). Although some products are known to be potential aerosol precursors, very little information has been published regarding the capacity to form particles. In fact, experiments carried out by our group using a high-volume photo-reactor with a natural sunlight source were the first to demonstrate that benzene forms condensable material (Martin-Reviejo and Wirtz, 2005). Other researchers also confirmed SOA formation in a smaller smog chamber in the presence or absence of seed aerosol (Ng et al., 2007; Sato et al., 2010).

The physical and chemical description of benzene aerosol would help us to understand its atmospheric distribution, reactivity and toxicity. In this sense, the aerodynamic size, which is related to residence time and lung deposition, depends on both the density and the size distribution. These latter properties have direct effects on light scattering and human health, and

also influence radiative forcing balances. In the same sense, a large number of condensed compounds can be present in SOA at trace levels, and vary significantly in polarity, volatility and toxicity. From other aromatic hydrocarbons, we know that ketonic-compounds, hydroxyl-compounds and carboxylic acids are the most interesting compounds in SOA (Fisseha et al., 2004; Hamilton et al., 2005). However, the fingerprint information of benzene oxidation condensed products is nearly unknown (Sato et al., 2010).

Our work is focused on SOA formation and the effects of oxidation conditions that connect the physical parameters of aerosols with its chemical composition. A fully-equipped high-volume atmospheric reactor was used to reproduce the most representative daytime reaction – OH radical photo-oxidation -. Several methods were used to induce OH generation, comparing H_2O_2 photolysis (in absence of NO_x), the classic initial addition of NO and HONO photolysis (both low-NO_x conditions). In the absence of seed aerosols and close to realistic oxidative conditions – OH concentrations and natural sunlight-, the present study was divided into the characterization of aerosol physical properties and the determination of chemical composition. In addition, since the oxidation of benzene is a case of multigenerational chemistry, the photo-oxidations of phenol and catechol, the main degradation products of benzene/OH reaction, was also carried out.

2. EXPERIMENTAL SECTION

2.1 Simulation chamber

The experiments were carried out in the EUPHORE photoreactors (Valencia, Spain). These chambers consist of two half-spherical fluoropolymeric bags, each one of 200 m^3. Several measuring systems were integrated for monitoring precursor species, products and physical parameters. Supplementary Information 1 shows the chamber distribution of the instruments employed. Pressure, humidity and temperature were measured using a pressure sensor (Air-DB-VOC, Sirsa, Madrid, Spain) and a dew point hydrometer (TS-2, Walz, Effeltrich, Germany). The facility was equipped with a White-type mirror system coupled to a Fourier Transform Infrared spectrometer with MCT detector (Magna 550, Nicolet Instrument, Madison, USA). The benzene, phenol, catechol, 2-nitrophenol, 4-nitrophenol, formaldehyde, maleic anhydride, formic acid, nitric acid, ozone, glyoxal and HONO concentrations were recorded with an absorption path length of 553.5 m, a spectral resolution of 1 cm^{-1} and a time resolution of 10 min. An Eco Physics AG (AL-ppt-77312, Duernten, Switzerland), an API NO_x monitor (API200AU, Teledyne API, San Diego, USA) and an NO_x analyzer (ML9841A, Teledyne Monitor, Englewood, USA) were used for measuring NO, NO_2 and NO_x. The dilution process was determined using SF_6 as a tracer – with an average dilution rate of 7×10^{-6} s^{-1} -. Aerosol mass concentration was measured with two instruments. One was a scanning mobility particle

sizer (SMPS), model 3080 (TSI, Shoreview, USA). This system measured size distributions in the 11 – 982 nm diameter range in real time with a 5 min scan rate, and it provides aerosol concentrations assuming spherical shapes and multi-charge correction for the condensed organic material. Sheath and aerosol sampling flows were 4 L min^{-1} and 0.30 L min^{-1}, respectively. The other automated instrument was a tapered element oscillating monitor (TEOM) (model 1400a, Ruppercht and Patashnick, Albany, USA) with a 1 min scan rate and a sampling flow of 3 L min^{-1}.

2.2 Smog chamber experiments

2.2.1 Experimental set-up. Since reactor walls can be a source of gas and/or particles due to the off-gassing of compounds, preliminary tests are required before each run. A blank chamber experiment, described in Borrás and Tortajada-Genaro, 2011, was performed to assure the absence of possible artefacts, providing air that had non-detectable hydrocarbons, NO_x and particles - aerosol background of 0.010 ± 0.005 μg m^{-3} (60 part cm^{-3}) -. Specific experiments such as addition of seed aerosols and O_3/NO_3 reactions were performed for correcting aerosol wall losses and confirming that aerosol formation is not due to ozone/nitrate radicals.

2.2.2 Photo-oxidation experiments. The photoreactor was filled with air from a purification system which included absorption driers (HEA 1400, Zander, Essen, Germany) with a molecular sieve (ECO 30 % MOL 70 %, Sogimair, Barcelona, Spain). The experiments consisted of the photo-decomposition under dry conditions (< 2% RH, 295-298 K) in the absence of inorganic seed aerosol. Experimental conditions are shown in Table 1. Benzene, phenol and catechol were fed to the photoreactor via heated air stream (Volkamer et al., 2002). Regarding the induced routes, H_2O_2 was introduced in the chamber with a sprayer, NO was added at 20 ppbV min^{-1} from an NO calibration bottle (99.999 % of 5000 ppm) and HONO was generated by a liquid-phase reaction between a 0.5 % $NaNO_2$ solution and a 30 % H_2SO_4 solution and transferred directly into the chamber via a stream of purified air. Later, all the reactants were mixed for 10 min before exposing them to sunlight (JNO_2 ~7×10^{-3} s^{-1}). The onset of aerosol formation was considered to occur when the first significant particle concentration was registered (> $3\sigma_{background}$). The sunlight exposure was conducted until the aerosol mass was steady; after that, the house of the chamber was closed. Measurements then continued for at least two hours to observe the aerosol decay behaviour. Then, aerosol data was corrected by dilution process and wall losses calculated based on this period and specific reference aerosol experiments.

2.3 Aerosol analysis

Particles were collected at maximum aerosol formation, under a flow rate of 80 L min^{-1} for 1 h, on GF/A 47 mm quartz fibre filters (Whatman, Brentford, England) that had been pre-baked at 500 ºC for 12 h to avoid organic binders. After the filters were weighed on a microbalance (MC21S, Sartorius, Goettingen, Germany), they were kept in a freezer at – 4 ºC.

For the time-evolution experiment, five filters were sampled at 1.5 h -7 h after the sunlight exposure. The SOA analysis was similar to that previously described by Borras and Tortajada-Genaro, 2011. Briefly, the filter was sonicated with CH_2Cl_2/CH_3CN (1:1) and a derivatization with O-(2,3,4,5,6-Pentalfluorobenzyl)-hydroxylamine hydrochloride (PFBHA) plus diluted N-methyl-N-trimethylsilyltrifluoroacetamide (MSTFA) was carried out. Finally, it was injected in the gas chromatograph – mass spectrometer (GC-MS). TRACE-DSQ II GC-MS (Thermo Fisher Scientific, Waltham, MA, USA) was used with an RTX-5MS column of 30 m × 0.25 mm I.D × 0.25 μm film thickness. The response factor was obtained from standards provided by Sigma Aldrich (Steinheim, Germany) – or a similar molecule in the case of a tentative compound -.

3. RESULTS AND DISCUSSION

3.1 Gas-phase products and aerosol profiles

The typical profiles of benzene degradation under different initial oxidative conditions are shown in Figure 1. The average OH concentrations present in the chamber were calculated from the first-order decay of benzene, being ~1.1×10^7 and ~1.4×10^7 molecules cm^{-3} in the absence of NO_x and low-NO_x experiments, respectively. Realistic oxidative conditions were simulated since the concentrations were of the same order of magnitude as those found in urban plumes (10^6 -10^7 molecules cm^{-3}) (Martín-Reviejo and Wirtz, 2005). Thus, the main difference between the photo-oxidation modes was only the rate of OH formation – HONO >> NO > H_2O_2 -. The main gaseous products were phenol, ozone, catechol, formic acid, nitric acid and formaldehyde. Other minority gases were glyoxal, maleic anhydride, 4-nitrophenol and 2-nitrophenol (0.1-20 ppbV). Some of these products have also been detected in the photo-oxidation of other aromatic hydrocarbons (Olariu et al., 2002).

A significant amount of aerosol was obtained under our experimental conditions – large chamber, natural radiation and high precursor concentrations -, even in an atmosphere free of seeds. The nucleation step involved solely the appearance of new particles because the absence of seeds prevented an early gas-condensed phase partitioning of semi-volatile compounds on the particle surface. Thus, the SOA was the consequence of condensable organic compounds reaching their saturation point. In NO_x-absence experiments, the beginning of aerosol nucleation required a sunlight exposure time of 2.1 ± 0.6 h, while for initial-NO conditions, the delay was 1.1 ± 0.2 h. The existence of a delay (or induction period) between the start of oxidation and SOA formation has also been observed for other aromatic hydrocarbons (Bahreini, et al., 2005). Under the addition of HONO – fast OH generation -, aerosols were formed immediately after the exposition of the pollutant to sunlight radiation. The growth profile was studied because it is related with partitioning coefficient, vapor pressure or stoichiometric mass coefficients which are inputs in aerosol modeling. Significant differences were observed depending on the OH

source. The slowest aerosol growth process was for benzene/NO_x-absence experiments, reaching maximum formation 4 h after aerosol nucleation. However, under both low-NO_x conditions, the maximum was reached 2.5 h after the start of nucleation. Figure 2 shows the curves of the aerosol mass concentration as a function of the benzene reacted after the onset aerosol formation. A strong linear correlation (R^2> 0.99) was observed with slopes 0.03, 0.05 and 0.16 for the absence of NO_x and both low-NO_x conditions, respectively. The highest slope of HONO conditions involved the fastest formation of semi-volatiles and gas-condensed phase partitioning. When aerosol growth finished, the steady state was reached - aerosol concentration and particle size remained constant -, with the highest SOA concentrations being obtained for low-NO_x conditions. All results indicated that the SOA formation process is NO_x-dependent.

3.2 Aerosol yield

The aerosol yield describes the capacity to produce particles and it is associated with pollution reduction strategies and aerosol modeling. The most simplified way to calculate the aerosol yield (Y) is the equation developed by Odum et al., 1996.

$$Y = \frac{M_0}{\Delta HC} \quad [1]$$

where M_o (μg m^{-3}) is the aerosol mass concentration formed and ΔHC (μg m^{-3}) is the mass concentration of hydrocarbon reacted. Yields, reported in Table 1, were thus calculated using the precursor concentration from FTIR data and the aerosol concentration from corrected SMPS data between the start and the maximum of aerosol formation. The uncertainties of aerosol yield were lower than 5% due to the good accuracy and reproducibility of both methods. The first observation was that benzene photo-oxidations produced lower aerosol yield than substituted aromatic hydrocarbons. Secondly, the presence of NO_x increased the SOA formation from 1.6 % to 9.7 %. This increment differs from the studies performed by Ng et al. 2007. This could be explained by changes in peroxy radical chemistry, e.g., effect of aerosol seeds (Klotz et al., 2002).

Aerosol precursors were studied by comparing experiments under different oxidative conditions. Odum et al., 1996 proposed a semi-empirical model based on the absorptive gas-particle partitioning of semi-volatile products described by:

$$K_i = \frac{Fi}{A_i \times M_0} \quad [2]$$

$$Y = \sum_i M_0 \frac{\alpha_i K_i}{1 + K_i M_0} \quad [3]$$

F_i and A_i are the particle-phase and gas phase concentration of compound *i*, respectively. The coefficient K_i is the gas-particle partitioning equilibrium constant, and the coefficient α_i is the

mass-based gas-phase stoichiometric coefficients. These parameters are valid only under equilibrium conditions. For this, yields were determined at the end of the experiment, when the parent compounds finished reacting, conversion to secondary products was completed and equilibrium was reached.

Figure 3 plots the aerosol yields versus concentration formed by varying initial benzene and oxidative reagent. These data were fitted, at the 95% confidence level, to one or two-product absorptive gas-particle partitioning models, summarized in Table 2. The curve in the absence of NO_x was well described by one-product model, suggesting that only one surrogate product - or a combination of only a few intermediates with similar K_i values (Coeur-Tourneur et al., 2009) - could be sufficient to describe the SOA formation. The results at low-NO_x fitted with a two-product model, suggesting that two surrogate products can describe SOA formation, and indicating that the contribution of this second intermediate is relevant. The sum of both α-coefficients corresponds to high-limit aerosol yields under the selected oxidative condition and they were similar to the slopes of ΔM vs. ΔHC plots (Figure 2), demonstrating the consistency of our data. Furthermore, since the stoichiometric parameters changed with the oxidation conditions, the particle formation occurs via condensation of second-generation oxidation products and not through first-generation products, as discussed by Kroll and Seinfeld, 2005.

The values of α_i and K_i indicated the relative abundance and the nature of the intermediate SOA precursors, respectively. According to the results, a semi-volatile intermediate ($K \approx 0.03$) is the main SOA surrogate compound. A low-volatile intermediate ($K \approx 0.3$) was additionally produced at minor concentrations only in the presence of NO_x. The benzene aerosol precursors herein reported were consistent with those calculated for Song et al. 2005 and Ng et al., 2007 that also proposed a semi-volatile intermediate ($K_i < 0.01$-0.05) and a low-volatility intermediate ($K_i > 0.2$-0.4) for m-xylene photo-oxidation.

3.3 Aerosol size distribution and density

The particle size distributions versus time for benzene photo-oxidations are reported herein (Figure 4). The data came from experiments without aerosol seeds to avoid a biased growth. Size-resolved wall-loss corrections were not needed, since negligible variations were observed during filter sampling for particle number concentration. In all cases, the aerosol size distribution showed an initial growth, which increased the average particle diameter controlled by condensation or homogeneous/binary nucleation process. Then, as growth continued, the particle distribution moved to larger sizes. After this, significant differences were detected for the assayed conditions. In the absence of NO_x, aerosol dynamics were controlled through coagulation and/or evaporation of small particles combined by the condensation of semi-volatile compounds on the surface of these particles. The condensation was incessantly produced due to

the continuously OH formation into the system. However, in low-NO_x experiments, only coagulation process controlled the aerosol dynamics. In this case, larger particles were formed – due to the burst initial OH formation - increasing the range of particle sizes and decreasing the total number of particles. Since particle diameter is associated with aerodynamic properties, residence time, human lung deposition and respiratory diseases, critical particle sizes were specifically determined. Table 3 lists the smallest and largest particle diameter, and the central diameter at the maximum particle concentration. In all cases, particle diameters corresponded to the fine particle fraction (diameters < 450 nm). A lower particle number concentration and higher central diameter were found with decreasing NO_x concentrations.

Particle densities were determined from the aerosol mass linear regression slope as a function of aerosol volume; see Table 1. The absence of NO_x increased the density and formed fewer but bigger particles. Most of the papers dealing with other aromatic systems theoretically assumed an SOA density of 1 or 1.5 g cm^{-3}. Only Bahreini et al., 2005 and Sato et al., 2010 determined experimentally an SOA density of 1.4 g cm^{-3} for xylenes and 1.3 g cm^{-3} for different aromatic hydrocarbons, respectively. Our study demonstrates that SOA density is a function of the oxidant conditions and, thus, must be specifically selected in order to develop reliable aerosol models.

3.4 Chemical characterization of SOA

The most relevant organic constituents in SOA from aromatic hydrocarbons are carboxylic acids, hydroxyl-carbonyl compounds and nitro-compounds (Jang and Kamens, 2001 and Hamilton et al., 2005). For that, their determination by GC-MS and PFBHA-MSTFA derivatization was selected (Borrás and Tortajada-Genaro, 2011). Figure 5 shows the chromatogram of products from benzene photo-oxidation. A total of 27, listed in Supplementary Information 2, were found, most of them confirmed by standards. Tentative compounds were proposed on the basis of their ion fragments and chemical properties (retention time and expected polarity). In all cases, the chemical ionization-spectrum confirmed the molecular weight. SOA compounds were divided into ring-retaining and ring-cleavage products, as described in gas phase (Klotz et al., 2002).

The ring-retaining products were oxygenated or nitro substituted aromatic compounds. The total identified mass range was 0.03 %, 2.1 % and 2.3 % for SOA in the absence of NOx, initial NO and HONO conditions, respectively. Previous studies have reported similar results for SOA from toluene (Hamilton et al., 2005) and xylene (Bahreini et al., 2005). In our experiments, the main products identified were phenol, catechol, 1,3-dihydroxybenzene, 1,4-dihydroxybenzene, 1,3,5-trihydroxybenzene, 1,2,4-trihydroxybenzene, corresponding to 0.001 – 0.026 % of total SOA mass. Studies by Hamilton et al., 2005 and Jang and Kamens, 2001 reported similar methylated products in toluene SOA. Several nitro-substituted aromatics (4-

nitrophenol, 2-nitrobenzene-1,3-diol and 4-nitrobenzene-1,3-diol) were also determined, corresponding to 0.05 – 2.32 % of the total SOA mass. However, few nitro-substituted aromatics were found, as a consequence of the lower NO_x concentrations used, compared to those observed by Forstners et al., 1997 and Kleindienst et al., 2004.

The ring-cleavage products were multi-oxygenated compounds coming from the further oxidation of gaseous linear aldehydes. Their percentage in the total SOA mass ranged from 1.2 – 15.9 %. The dicarboxylic acids (C2-C6) were found as pairs of saturated and unsaturated homologues. Unsaturated compounds, generated as primary products, could form saturated products during the reaction. They represented 0.15 – 2.6 % of total SOA, with succinic acid being the most abundant. These products are analogues of the multifunctional carboxylic acids identified by Jang and Kamens, 2001, Sato et al., 2007 and Fisseha et al., 2004 in the photo-oxidations of toluene and 1,3,5-trimethylbenzene. Moreover, oxalic, malonic and succinic acids were quantified in a similar total SOA mass (0.1 – 2.6 %). The detection of trans-trans-muconic acid and its isomers deserves special emphasis (0.1 – 0.4 %). They are degradation products of muconaldehyde, which has been proposed as an important SOA precursor (Martin-Reviejo and Wirtz, 2005; Sato et al., 2010). Nevertheless, neither this gaseous aldehyde nor most of its condensed products had previously been detected during any aromatic hydrocarbon photo-oxidations. Only muconic acid was previously detected in the SOA of toluene photo-oxidation (Sato et al., 2007). For this reason, our quantification of structurally defined muconic acid is an important result for the understanding of the degradation mechanism. The oxidation of muconaldehyde explained the presence of compounds such as the C6-unsaturated keto-hydroxyl-compound ($C_6H_8O_2$), C6-unsaturated dihydroxyl-compound ($C_6H_{10}O_2$) and C6-unsaturated hydroxyl-carboxylic acid ($C_6H_8O_3$). Other multi-oxygenated compounds were tentatively identified (0.2 – 1%), such as C4-keto-carboxylic acid, C3-hydroxyl-carboxylic acid, C2-hydroxyl-carboxylic acid, C5-keto-hydroxyl compound, C5-unsaturated keto-hydroxyl compound, C4-unsaturated hydroxyl-carboxylic acid, C5-unsaturated keto-carboxylic acid and C5-unsaturated dicarboxylic acid. Finally, glyoxal and methyl-glyoxal were detected, probability from the cleavage of condensed polymeric or oligomeric compounds.

Most molecules were detected in all oxidant conditions, but the differences in terms of concentration were not negligible. In general, the presence of OH radicals alone improves the formation of ring-cleavage aerosol products (52.5 $\mu g\ m^{-3}$ in absence NO_x and 1.5 - 33.5 $\mu g\ m^{-3}$ for low-NO_x reactions). The most relevant decrease of concentrations in the presence of NO_x was observed for C4-dicarboxylic acids. The exception is trans-trans-muconic acid presented the maximum concentration under HONO conditions. Meanwhile, the presence of both NO_x and OH oxidants increases the formation of ring-retaining products (0.1 to 17 $\mu g\ m^{-3}$). Some of these products were nearly constant, but the formation of 4-nitrophenol, 4-nitrobenzene,1-2-diol was only observed under the presence of NO_x.

Globally, multi-oxygenated compounds comprised from 2.3 – 12 % of the total aerosol mass. These values are in the same order as those reported by Sato et al., 2007 for toluene photo-oxidation. The identified percentage increased to 3 – 21 % if the tentative degradation products were included – unknown compounds are not taken into account -. Additionally, the total aerosol mass identified was lower in the presence of NO_x. This could be explained by the formation of organic nitrates and acylperoxy nitrates which increase SOA formed but were not determined herein.

Figure 6 shows the temporal evolution of the concentrations of relevant condensate products. At first, the concentrations increased significantly, but later they kept roughly constant for most organic multi-oxygenated compounds. In contrast, the concentrations of nitro-compounds (4-nitrobenzene-1,4-diol, 2-nitro-1,3-benzene diol and 4-nitrophenol) decreased at the end of the experiment. The identified fraction was lower at the end than at the beginning of the experiment. This can be explained by the formation of polymers, other organic nitrates and acylperoxy nitrates owing to the coagulation aerosol processes or due to the follow photolysis or photo-oxidation of nitro-compounds formed.

3.5 Multigenerational studies

Benzene/phenol/catechol oxidations can be considered multigenerational system that acts as SOA precursor (Kroll et al., 2008). The benzene/OH reaction produces phenol and the formation of catechol can be explained by starting from the OH/phenol adduct and H-abstraction by O_2. For this, the photo-oxidations of phenol (first-generation) and catechol (second-generation) were compared with those of benzene.

Firstly, we analyzed the benzene oxidation and the yields of its hydroxylated products (Φ) were calculated according to:

$$\Phi = \frac{k_{OH}(product) \times [product] \times fc}{k_{OH}(precursor) \times [precursor]} \qquad [4]$$

Under the presence of NO_x, the phenol yield was obtained with $k_{OH}(phenol) = 2.63\times10^{-11}$ cm^3 s^{-1}, $k_{OH}(benzene) = 1.23\times10^{-12}$ cm^3 s^{-1}, (Volkamer et al. 2002), [product] and [precursor] the measured concentrations of phenol and benzene at steady state, respectively, with f_c being the correction factor obtained during the set-up of the phenol experiments. However, for experiments under the absence of NO_x, where phenol concentrations increased continuously, [precursor] was calculated as increment at the early state of the reaction. The Φ-values were 53 ± 4 % and 38 ± 2 %, respectively. These results - yields and NO_x dependence - agree with those obtained in the exhaustive study performed by Volkamer et at., 2002. Catechol yields were calculated at steady state (eq. 4), considering $k_{OH}(catechol) = 1.04\times10^{-10}$ cm^3 s^{-1} (Olariu et al., 2002), being 75 ± 4 % in the absence of NO_x, and 8 ± 0.4 % for low-NO_x conditions. Similar

high yields of catechol in the absence of NO_x have been described by Olariu et al., 2002; Berndt et al., 2003 and Volkamer et al., 2002. Therefore, NO_x reduced the formation of monohydroxy and dihydroxy-compounds.

Secondly, we studied phenol photo-oxidations. The main products were catechol, ozone, formic acid and nitric acid. The catechol yields herein, at the steady-state assumption (eq. 4), were around 80 % in the absence of NO_x conditions, and 20 % for the low-NO_x conditions. These catechol yields agree with the results obtained by Berndt and Böge, 2003, i.e., around 75 % at 295 K and a decreased catechol yield in the presence of NO_x (35%).

Thirdly, we found that the catechol/NO_x reaction produced ozone, formic acid and nitric acid. The main difference was that catechol totally reacted after a sunlight exposition of 1.5h, confirming that catechol is much more reactive than phenol or benzene. These results agree with the in-depth atmospheric degradation studies described by Olariu et al., 2002.

The comparison of three experimental series reveals the important effect of NOx concentration and the existence of secondary reactions that affect only benzene. As an explanation, the OH-adduct/O_2 reaction was proposed and expected to affect the degradation routes leading to ring-retaining products. In this sense, Volkamer et al., 2002 proposed several pathways for benzene degradation in which phenol is not involved, such as the formation of benzene oxide/oxepin. There may also be other channels that are NO_x-dependent and dominant under atmospheric conditions, leading to the formation of epoxide-type compounds and further ring-cleavage products. For benzene and toluene series, Olariu et al., 2002 already observed that the dihydroxycompound yields in the OH reaction with monohydroxycompounds were much higher than the hydroxycompound yields with parent compounds.

Regarding SOA formation, Table 1 shows the aerosol yield increasing with the oxidation state (catechol >> phenol > benzene). A similar trend is obtained from the aerosol growth curve (ΔM vs ΔHC), plotted in Figure 7. A strong linear correlation ($R^2 > 0.99$) was observed with slopes (upper-limit aerosol yield) of 0.09, 0.19 and 0.48 for benzene, phenol and catechol, respectively. According to Kroll et al., 2008, this linear aerosol growth describes the situation of a multigenerational system where the products have a faster oxidation reaction with a higher yield than their parents. In conclusion, the results confirmed that the primary and secondary degradation products are progressively greater SOA precursors than benzene. Moreover, the aerosol maximum mass concentration, density and particle size distribution of phenol SOA and catechol SOA are listed in Table 1 and 3.

The chemical characterization of SOA from phenol and catechol photo-oxidations was studied (Supplementary Information 2). Similar products to those observed from benzene photo-oxidation were detected. C4-dicarboxylic acid and their unsaturated isomers, trans,trans-muconic acid and their isomers, multi-oxygenated and nitro-aromatic compounds were the most significant products. Specific products of phenol or catechol photo-oxidations were longer

hydroxyl-carbonyl compounds and multi-substituted nitro-aromatic compounds. In conclusion, the results confirmed that the formation reactions are quite similar between these serial OH-aromatic hydrocarbons; the difference is in the mass produced but not in the SOA composition. Although Nakao et al., 2010 reported SOA formation from phenolic compounds under the absence of NO_x, it is worthy of mentioning that both the physical and chemical properties of particles from phenol photo-oxidations have been firstly reported.

3.6 Mechanistic interpretation

The advances in the understanding of benzene photo-oxidation, particularly the formation of gas-phase products, were reviewed by Volkamer et al., 2002. The present study, focused on the condensed phase, has found that the rate of OH radical generation and the NO_x presence produce a great variation in SOA, as occurs in the gas phase. The rapid photolysis of HONO (1.44×10^{-3} s^{-1}) and OH generation promoted an immediate SOA formation which was continued by the radicals produced through recycling via NO_x/HO_x chemistry. The radical source in the initial-NO experiments came from a heterogeneous reaction of NO_2 on the chamber wall (Ng, et al. 2007), promoting a slower OH generation and a lower SOA production. The slowest, although roughly constant, OH generation derived from the photolysis of H_2O_2 (6.04×10^{-6} s^{-1}), producing the slowest and smallest SOA formation. For this reason, differences in observed SOA are presumably linked to differences in gas-phase chemistry. Two general aerosol formation routes of benzene photo-oxidation can be suggested; see Figure 8. Route A involves the formation of phenol, promoting the formation of SOA intermediate 1. Route B, directed by nitrogen oxides, produces a gaseous intermediate, perhaps a ring fragmentation product such as muconaldehyde. This intermediate also induces the aerosol formation. Hydroxyperoxides, which are promoters of condensed products such as the alkoxy radical, the organic nitrates, alcohols and carbonyl compounds, can be formed during both of these multi-step routes (Kroll and Seinfeld, 2008).

Physical properties, chemical composition and multigenerational studies have confirmed the reactions discussed. Firstly, the proposed routes explain why benzene SOA formation is similar to its hydroxylated products but with a delay. Although these products react faster than do their parent hydrocarbons – k_{OH}(benzene) < k_{OH}(phenol) << k_{OH}(catechol) -, condensed products are generated through the same SOA intermediates. Secondly, the inverse relationship between phenol yield and SOA formation is justified by the enhancing effect caused in route B by NO_x. This behavior is in good agreement with Olariu et al., 2002, who previously affirmed that the VOC/NO_x reaction becomes competitive with other oxidative atmospheric species, opening reaction pathways that most likely lead to a different product distribution. Moreover, Kroll and Seinfeld, 2008, showed that the presence of NO_x may impact on the heterogeneous reactions. Thirdly, the proposed pathway is also consistent with our

445 available data on the NO_x effect. Aerosol properties change when NO_x concentrations increase,
446 since the formation reactions of both aerosol precursors are activated (route A) or induced (route
447 B) by NO_x. This assumption is reinforced by the fact that different benzene consumptions, gas-
448 phase product yields, aerosol physical properties (yield, distribution, density) and chemical
449 composition were registered.
450

451 ## *5. CONCLUSIONS*

452 This study is the first to carry out an in-depth interpretation of the relationships between
453 the oxidant conditions in benzene photo-oxidations and the properties of the aerosol produced.
454 We propose that the formation of aerosol precursors is a function of the relative importance of
455 two reaction channels controlled by NO_x-concentration. The analysis of aerosol parameter
456 yields and condensed products has provided us with information on the nature of both SOA
457 precursors. As a result, all the physical properties and chemical composition here determined for
458 benzene SOA are strongly NO_x-dependent. This conclusion is reinforced by the SOA yield, the
459 particle size distribution and the density of the phenol photo-oxidations which showed the same
460 behavior. The mutigenerational studies confirmed the generation of the same gas-phase and
461 SOA products, although produced at different ratios as a function of NO_x presence. Taking into
462 account the emission factors, the SOA formed from benzene-phenol-catechol/OH reactions is
463 expected to be significantly found in the urban environment, presenting important atmospheric
464 implications.
465

466 ## *ACKNOWLEDGEMENTS*

467 The authors wish to thank J.T.B, Martin-Reviejo, the Spanish Ministry of Science and
468 Technology IMSEUR project (Project nº REN2002-01484/CLI). The Instituto Universitario
469 CEAM-UMH is partly supported by Generalitat Valenciana, Fundación Bancaja, and the
470 projects GRACCIE (Consolider-Ingenio 2010) and FEEDBACKS (Prometeo-GVA).
471

472 **REFERENCES**

473 1. Bahreini, R., Keywood, M.D., Ng, N.L., Varutbangkul, V., Gas, S., Flagan, R.C.,
474 Seinfeld, J.H., Worsnop, D.R., Jimenez, J.L., 2005. Measurements of secondary organic
475 aerosol from oxidation of cycloalkenes, terpenes, and m-xylene using an aerodyne
476 aerosol mass spectrometer. Environmental Science and Technology 39, 5674-5688.
477 2. Berndt, T., Böge, O., 2001. Gas-phase reaction of OH radicals with benzene: products
478 and mechanism. Physical Chemistry Chemical Physics 3, 4946-4956.
479 3. Berndt, T., Böge, O., 2003. Gas-phase reaction of OH radicals with phenol. Physical
480 Chemistry Chemical Physics, 5, 342-350.

4. Berndt, T., Böge, O., 2006. Formation of phenol and carbonyls from the atmospheric reaction of OH radicals with benzene. Physical Chemistry Chemical Physics 8, 1205-1214.
5. Borrás, E., Tortajada-Genaro, L.A., 2011. Determination of oxygenated compounds in secondary organic aerosol from isoprene and toluene smog chamber experiments. International Journal of Environmental Analytical Chemistry, DOI 10.1080/03067319.2011.572164.
6. Coeur-Tourneur. C., Tomas, A., Guilloteau, A., Henry. F., Ledoux, F., Visez, N., Riffault, V., Wenger, J.C., Bedjanian, Y., 2009. Aerosol formation yields from the reaction of catechol with ozone. Atmospheric Environment 43, 2360-2365.
7. Finlayson-Pitts, B.J.; Pitts J.N., 2002. Chemistry of the Upper and Lower Atmosphere: Theory, Experiments and Applications. Academic Press, San Diego, CA.
8. Fisseha, R., Dommen, J., Sax, M., Paulsen, D., Kalberer, M., Maurer, R., Höfler, F., Weingarther, E., Baltensperger, U., 2004. Identification of Organic Acids in Secondary Organic Aerosol and the Corresponding Gas Phase from Chamber Experiments. Analytical Chemistry 76, 6535-6540.
9. Forstner, H.J.L., Flagan, R.C., Seinfeld, J.H., 1997. Secondary organic aerosol from the photo-oxidation of aromatic hydrocarbons: Molecular composition. Environmental Science and Technology 31, 1345-1358.
10. Hamilton, J.F., Webb, P.J., Lewis, A.C., M-Reviejo, M., 2005. Quantifying small molecules in secondary organic aerosol formed during the photo-oxidation of toluene with hydroxyl radicals. Atmospheric Environment 39, 7263–7275.
11. Jang, M.S., Kamens, R.M., 2001. Characterization of secondary aerosol from the photooxidation of toluene in the presence of NOx and 1-propene. Environmental Science and Technology 35, 3626–3639.
12. Kalberer, M., Paulsen, D., Sax, M., Steinbacher, M., Dommen, J., Prevot, A.S.H., Fisseha, R., Weingartner, E., Frankevich, V., Zenobi, R., Baltensperger, U., 2004. Identification of Polymers as Major Components of Atmospheric Organic Aerosols. Science 303, 1659-1662.
13. Kleindienst, T.E., Conver, T.S., McIver, C.D., Edney, E. O 2004. Determination of Secondary Organic Aerosol Products from the Photooxidation of Toluene and their Implications in Ambient PM2.5. Journal of Atmospheric Chemistry 47, 79–100.
14. Klotz, B., Volkamer, R., Hurley, M.D., Sulbaek Andersen, M.P., Nielsen, O.J., Barnes, I., Imamura, T., Wirtz, K., Becker, K.H., Platt, U., Wallington, T. J., Washida, N., 2002. OH-initiated oxidation of benzene. Part II. Influence of elevated NOx concentrations. Physical Chemistry Chemical Physics 4, 4399-4411.

15. Kroll, J.H., Seinfeld, J.H., 2005. Representation of secondary organic aerosol laboratory chamber data for the interpretation of mechanism of particle growth. Environmental Science and Technology 39, 4159-4165.
16. Kroll, J.H., Seinfeld, J.H., 2008. Chemistry of secondary organic aerosol: Formation and evolution of low-volatility organics in the atmosphere. Atmospheric Environment 42, 3593-3624.
17. Martin-Reviejo, M., Wirtz, K., 2005. Is benzene an aerosol precursor? Environmental Science and Technology 39, 1045-1054.
18. Nakao, S., Clark, C., Tang, P., Sato, K., Cocker III, D., 2011. Secondary Organic Aerosol formation from phenolic compounds in the absence of NOx. Atmospheric Chemistry and Physics Discussions, 11, 2025 – 2055.
19. Ng, N.L., Kroll, J.H., Chan, A.W.H., Chhabra, P.S., Flagan, R.C., Seinfeld, J.H., 2007. Secondary organic aerosol formation from m-xylene, toluene and benzene. Atmospheric Chemistry and Physics 7, 3909-3922.
20. Odum, J.R., Hoffmann, T., Bowman, F.M., Collins, D., Flagan, R.C., Seinfeld, J.H., 1996. Gas/particle partitioning and secondary organic aerosol yields. Environmental Science and Technology 30, 2580–2585.
21. Olariu, R.I., Klotz, B., Barnes, I., Becker, K.H., Mocanu, R., 2002. FT-IR study of the ring-retaining products from the reaction of OH radicals with phenol, o-, m-, and p-cresol. Atmospheric Environment 36, 3685-3697.
22. Raoult, S., Rayez, M-T., Rayez, J-C., Lesclaus, R., 2004. Gas phase oxidation of benzene: Kinetics, thermochemistry and mechanism of initial steps. Physical Chemistry Chemical Physics 6, 2245-2253.
23. Sato, K., Hatakeyama, S., Imamura T., 2007. Secondary Organic Aerosol Formation during the Photooxidation of Toluene: NOx Dependence of Chemical Composition. The Journal of Physical Chemistry A, 111, 9796-9808.
24. Sato, K., Takami A., Isozaki, T., Hikida, T., Shimono, A., Imamura, T., 2010. Mass spectrometric study of secondary organic aerosol formed from the photo-oxidation of aromatic hydrocarbons. Atmospheric Environment 44, 1080-1087.
25. Song, C., Na, K., Cocker III, D.R., 2005. Impact of the hydrocarbon to NOx ratio on secondary organic aerosol formation. Environmental Science and Technology 39, 3143-3149.
26. Volkamer, R., Klotz, B., Barnes, I., Imamura, T., Wirtz, K., Washida, N., Becker, K.H., Platt,U., 2002. OH-initiated oxidation of benzene; part I. Phenol formation under atmospheric conditions. Physical Chemistry Chemical Physics 4, 1598-1610.

553 **FIGURE AND TABLE CAPTIONS**

554 Figure 1. Reaction profiles: (a) low-NO_x experiment (12800 μg m^{-3} benzene, 17 ppm H_2O_2), (b)
555 low-NO_x experiment (3030 μg m^{-3} benzene, 100 ppb NO), c) low-NO_x experiment (6150 μg m^{-3}
556 benzene, 75 ppb HONO).

557 Figure 2. Plot of aerosol mass concentration against the reacted benzene concentration from the
558 onset aerosol formation.

559 Figure 3. Aerosol yield curves from benzene reactions: (a) absence-NO_x experiments, b) low-
560 NO_x experiments (initial NO) and (c) low-NO_x experiments (HONO).

561 Figure 4. Particle size distribution in benzene photo-oxidation reactions: a) absence-NO_x
562 experiment b) low-NO_x experiment (5300 μg m^{-3} benzene, 75 ppb HONO).

563 Figure 5. Chromatogram of the m/z 73+181 from an aerosol sample obtained from
564 benzene/HONO photo-oxidation.

565 Figure 6. Temporal evolution of the main benzene photo-oxidation SOA products under low-
566 NOx conditions (3256 μg m^{-3} benzene, 150 ppb HONO).

567 Figure 7. Plot of aerosol mass concentration against the reacted VOC concentration during
568 aerosol growth. Benzene experiment (16900 μg m^{-3}, 75 ppb oHONO), phenol experiment (1500
569 μg m^{-3}, 75 ppb HONO) and catechol experiment (1970 μg m^{-3}, 250 ppb of HONO).

570 Figure 8. Hypothetical proposed degradation routes.

571 Table 1. Experimental conditions of photo-oxidation reactions.

572 Table 2. Aerosol yield parameters determined for the benzene data set: (a) absence-NO_x
573 experiments, (b) low-NO_x experiments.

574 Table 3. Characteristic size and number concentration of particles.

575 Supplementary information 1. Instrumentation facilities in EUPHORE chamber.

576 Supplementary information 2. Concentrations (μg m^{-3}) of multi-oxygenated organic compounds
577 identified in benzene, phenol and catechol photo-oxidations.

578

579

Code	Aromatic hydrocarbon	HC ($\mu g\ m^{-3}$)	H_2O_2 (ppbV)	NO (ppbV)	HONO (ppbV)	O_3 (ppbV)	ratio ppbC/ppbNOx	ΔHC ($\mu g\ m^{-3}$)	Y (%)	ρ ($g\ cm^{-3}$)
1	Benzene	6750	12000	-	-	-	-	1855	1.6	1.5
2	Benzene	8330	12000	-	-	-	-	1835	2.6	n.a
3	Benzene	12800	17000	-	-	-	-	2340	2.6	1.5
4	Benzene	8320	17000	-	-	-	-	2525	2.9	n.a
5	Benzene	3030	-	100	-	-	57	1260	3.4	n.a
6	Benzene	6000	-	45	-	-	251	2400	3.8	n.a
7	Benzene	8540	-	46	-	-	349	1665	2.6	1.3
8	Benzene	12600	-	43	-	-	551	2040	3.3	1.4
9	Benzene	3256	-	-	150	-	41	430	5.8	1.1
10	Benzene	3520	-	-	75	-	88	330	2.8	n.a
11	Benzene	6150	-	-	75	-	154	1170	7.0	1.1
12	Benzene	12170	-	-	75	-	305	1390	9.7	1.3
13	Benzene	16900	-	-	75	-	424	2250	8.6	1.1
14	Phenol	1325	17000	-	-		-	805	12.8	1.4
15	Phenol	1500	-	-	75		31	870	18.0	1.3
16	Catechol	1915	17000	-	-		-	1915	45.0	1.3
17	Catechol	1970	-	-	35		10	1970	53.0	1.2

580 Table 1. n.a : not available

581 Standard error < 5%

582

583

584

585

	α_1	α_2	K_1	K_2	R^2
One-product model					
Absence-NOx	0.045	-	0.024	-	0.981
Initial-NO	0.053	-	0.024	-	0.952
Low-NOx (HONO)	0.112	-	0.024	-	0.974
Two-product model					
Absence-NOx	0.043	0.008	0.022	0.091	0.926
Low-NOx (Initial-NO)	0.046	0.02	0.007	0.105	0.954
Low-NOx (HONO)	0.076	0.035	0.016	0.118	0.973

Table 2

Code	Smallest diameter (nm)	Largest diameter (nm)	Central diameter (nm)	Concentration (part cm^{-3})
1	13	414	241	43162
2	14	429	269	11229
3	39	385	233	45262
4	20	429	102	202815
5	16	400	106	18867
6	21	419	118	73758
7	12	346	79	192764
8	22	322	122	192801
9	35	445	110	195236
10	26	395	104	178569
11	48	311	106	168503
12	18	445	146	127772
13	45	414	141	153066
14	59	300	157	222111
15	15	400	126	247941
16	45	445	235	764892
17	18	496	195	764098

Table 3

614 Figure 1

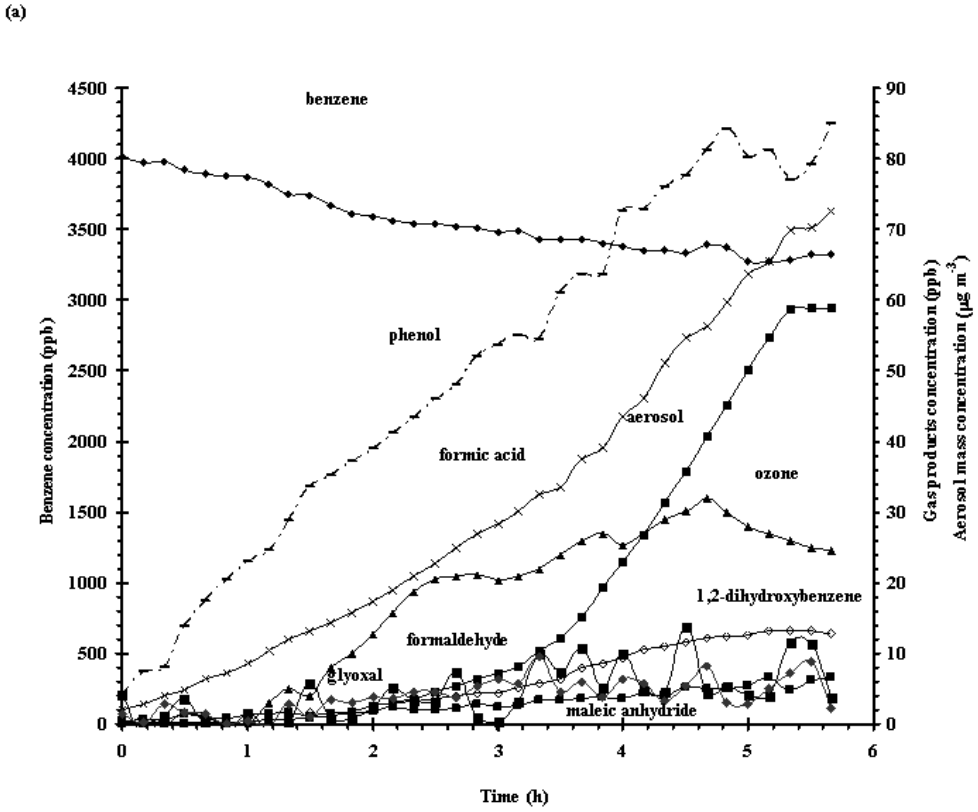

615

616

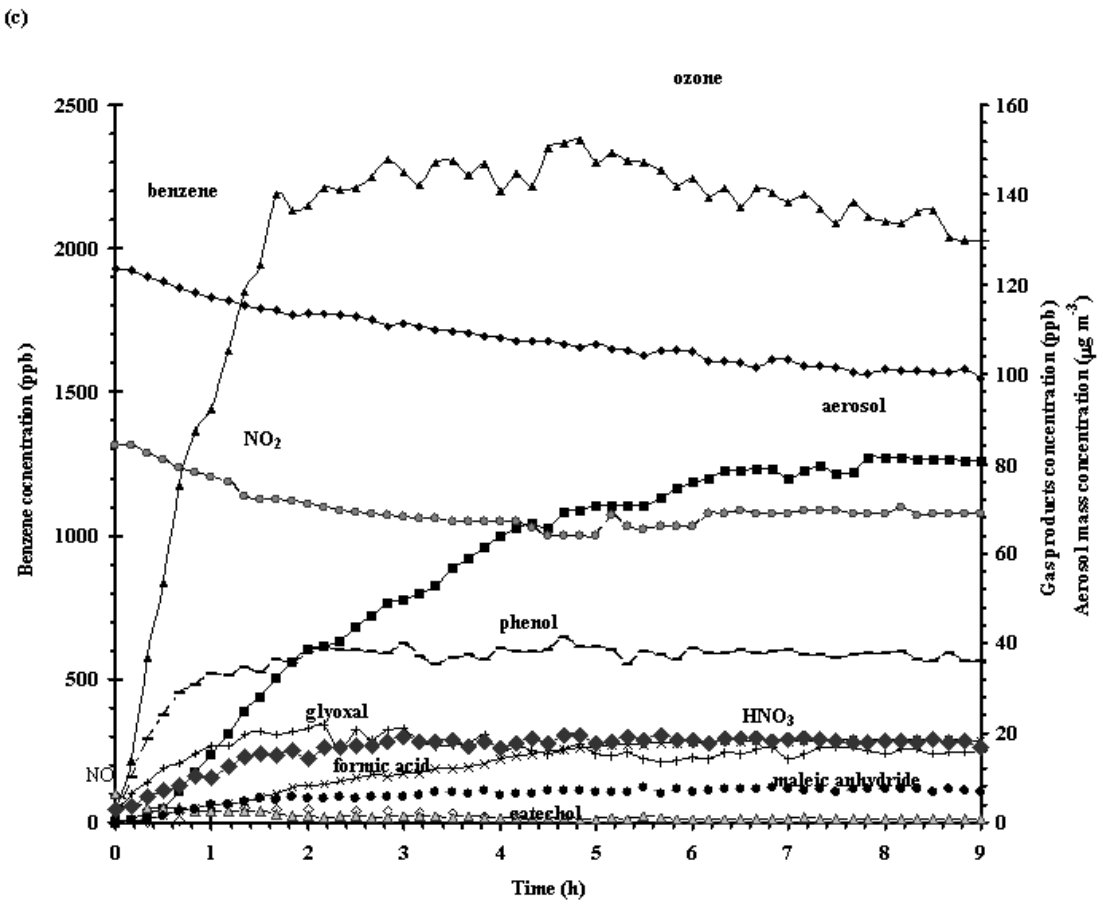

617
618 Figure 2

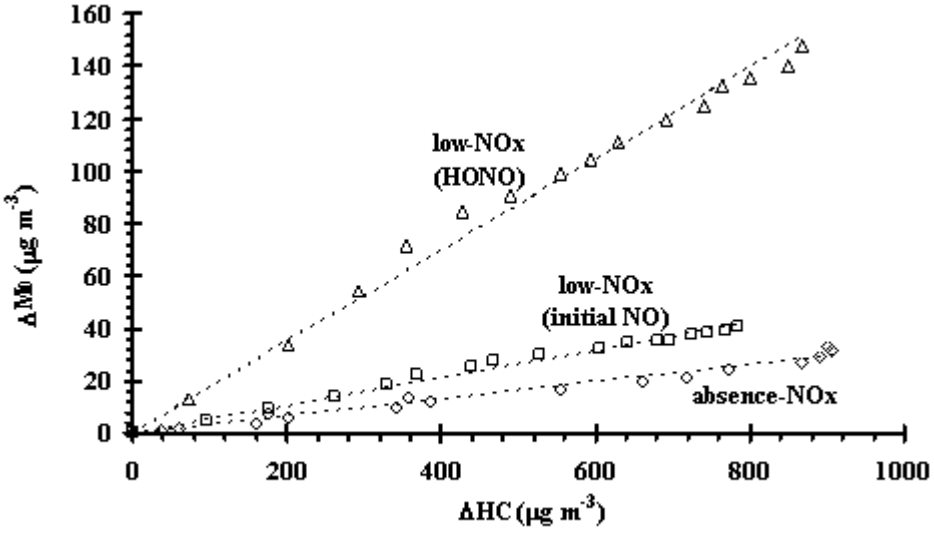

619
620
621
622
623 Figure 3

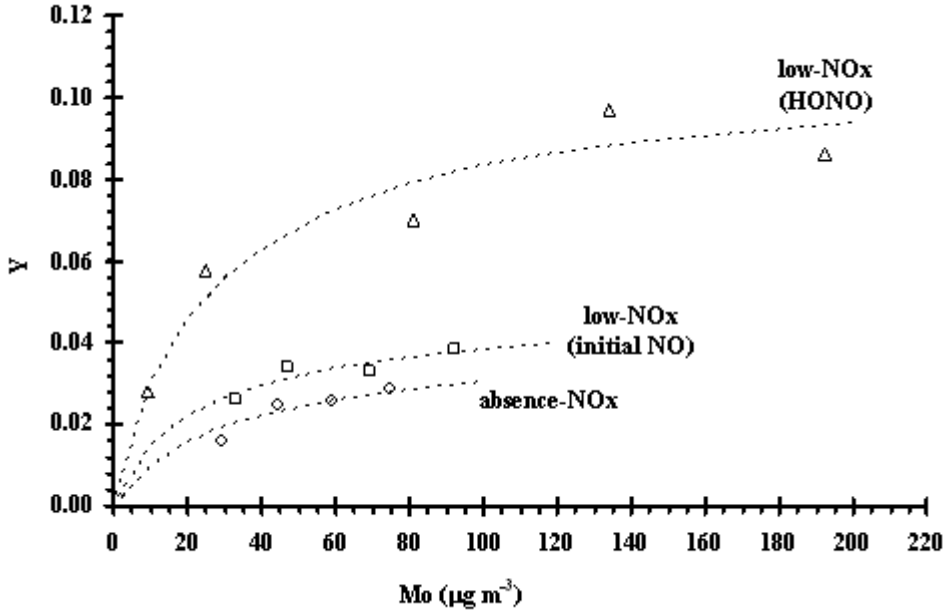

624

625 Figure 4

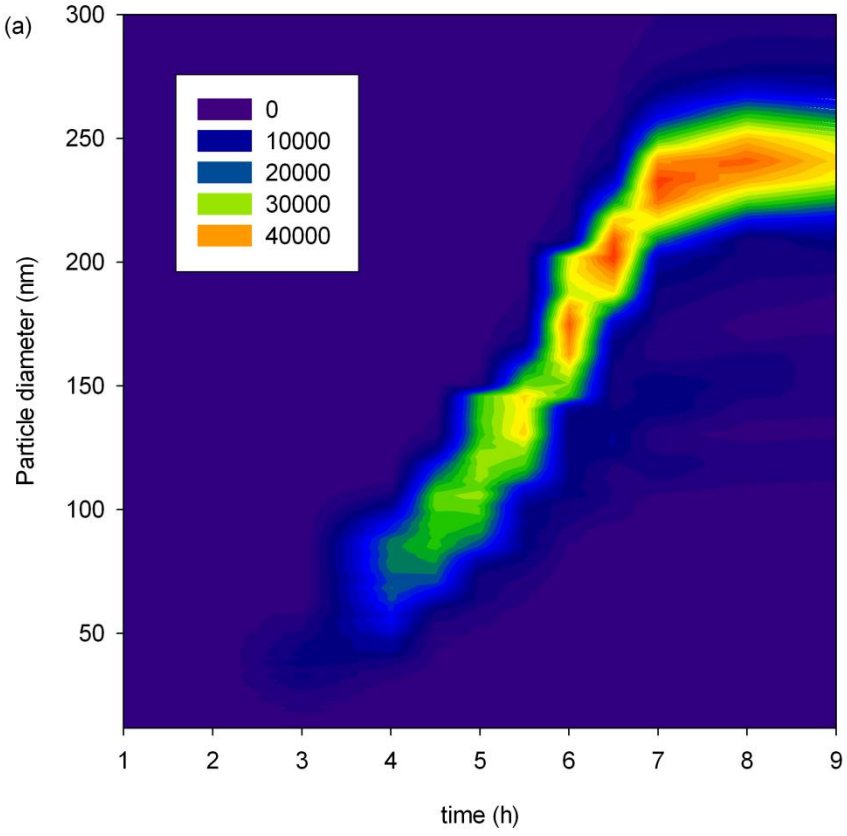

626

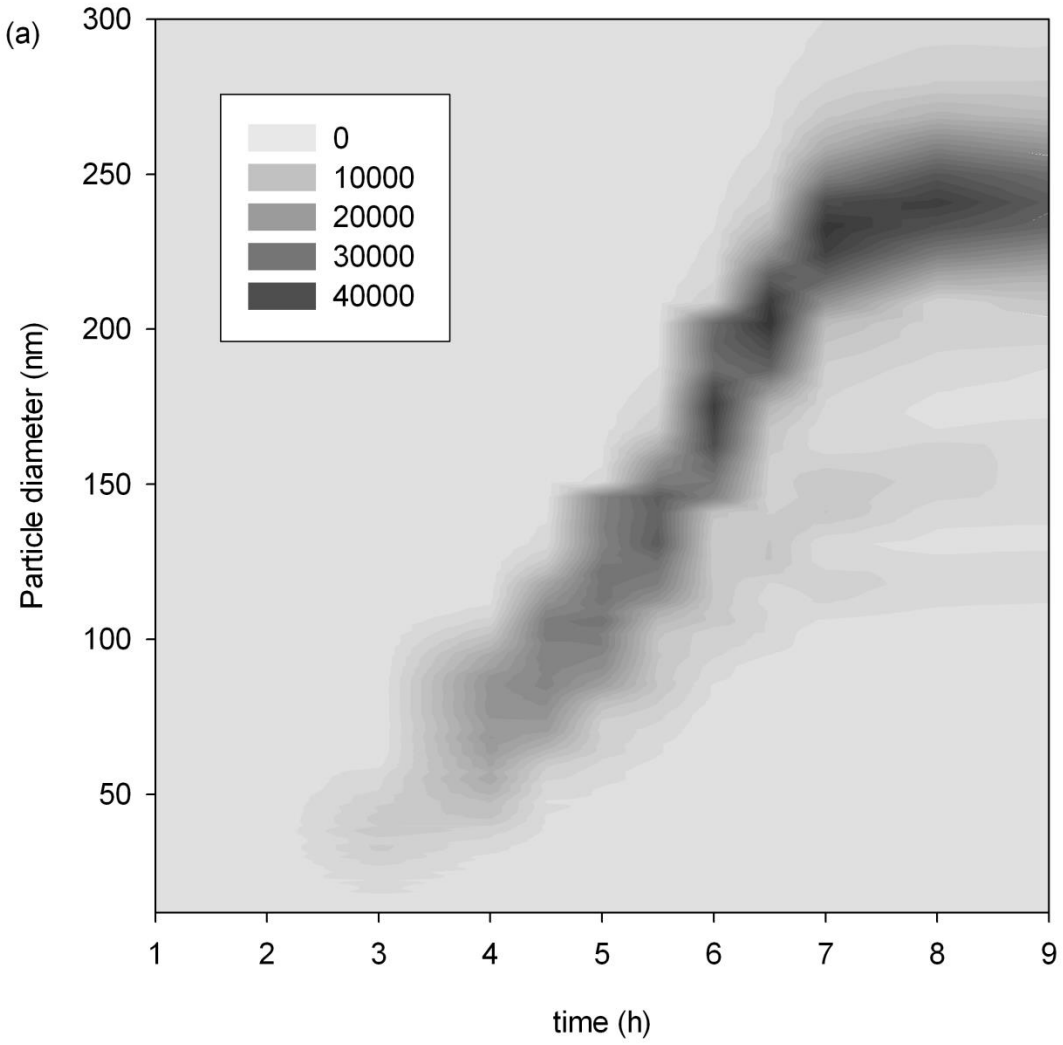
(a)
300
250
200
150
100
50
Particle diameter (nm)
0
10000
20000
30000
40000
1
2
3
4
5
6
7
8
9
time (h)

627

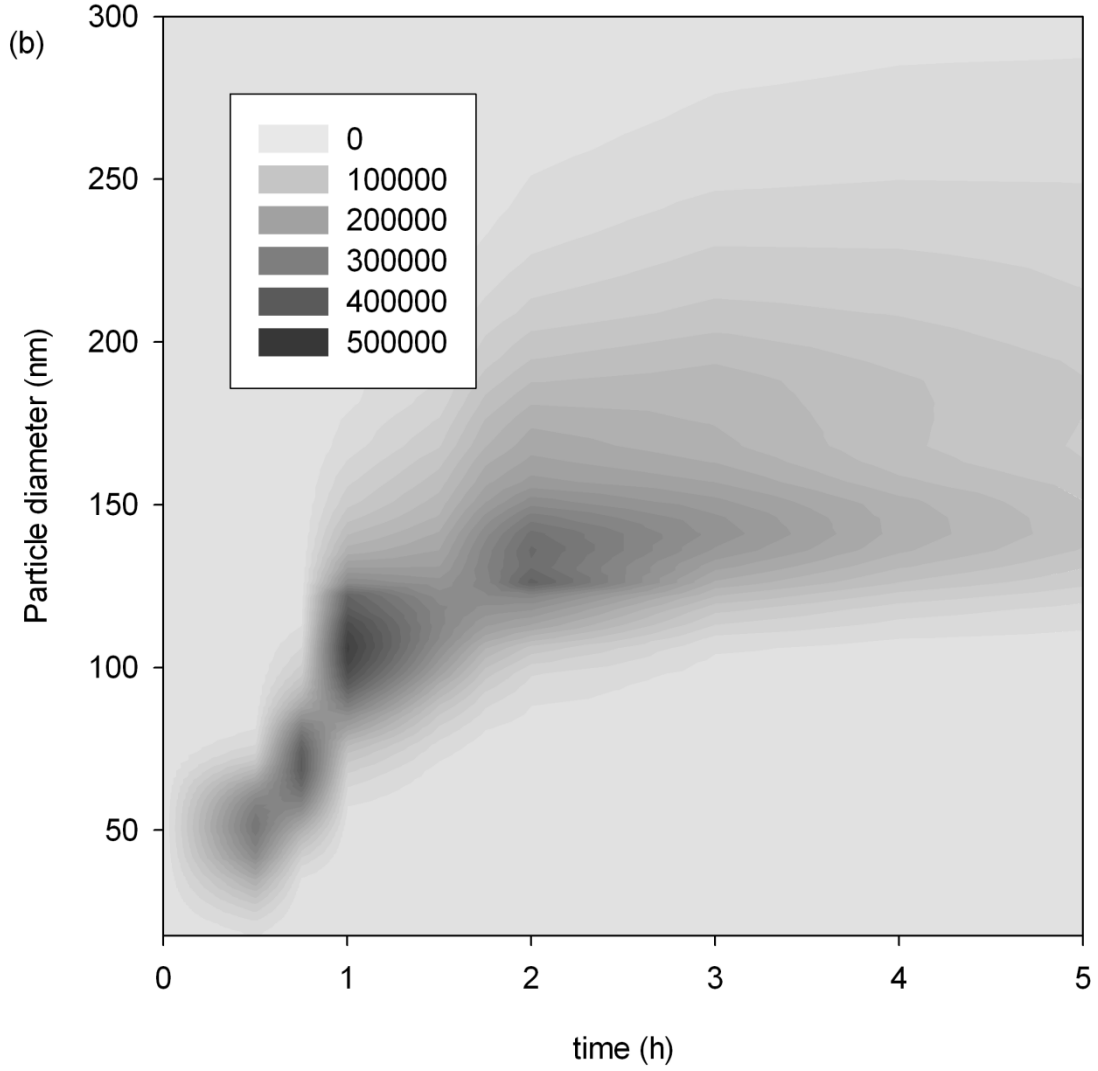

628

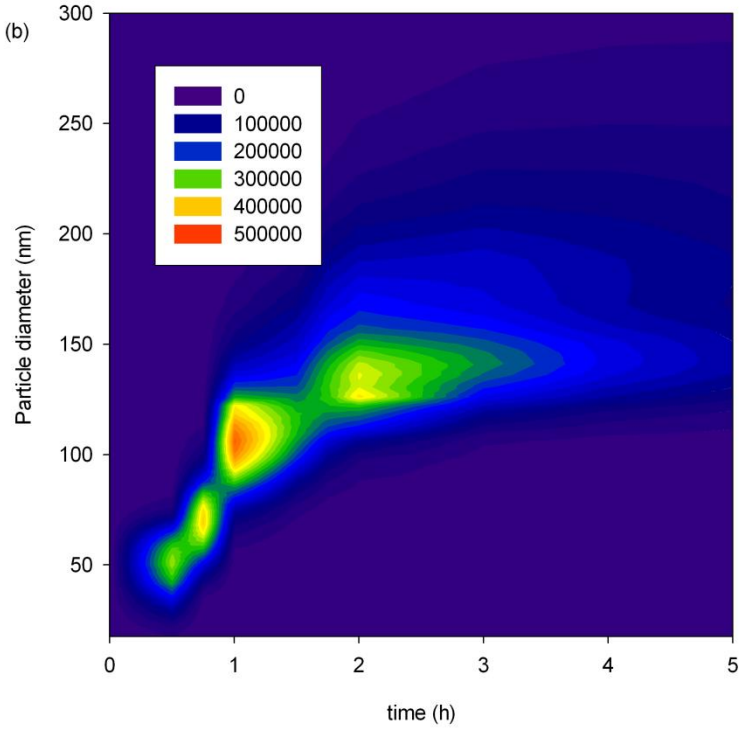

629

Figure 5

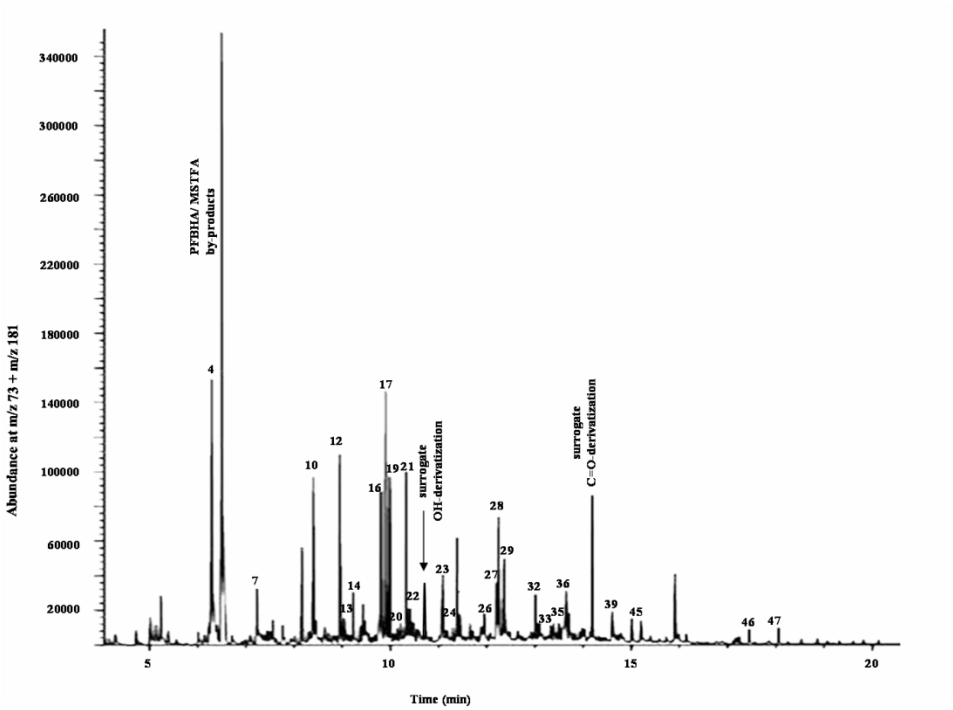

630

631 Figure 6

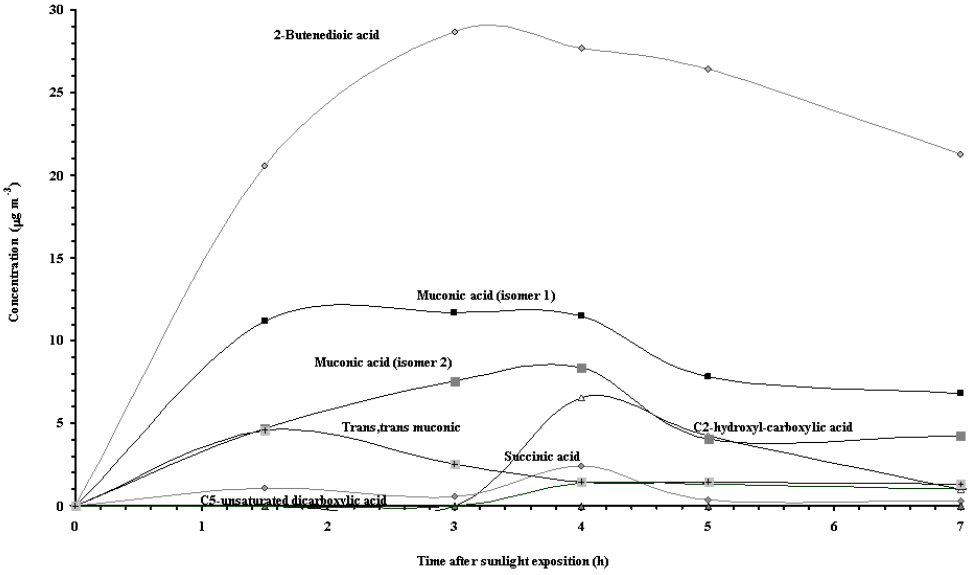

632

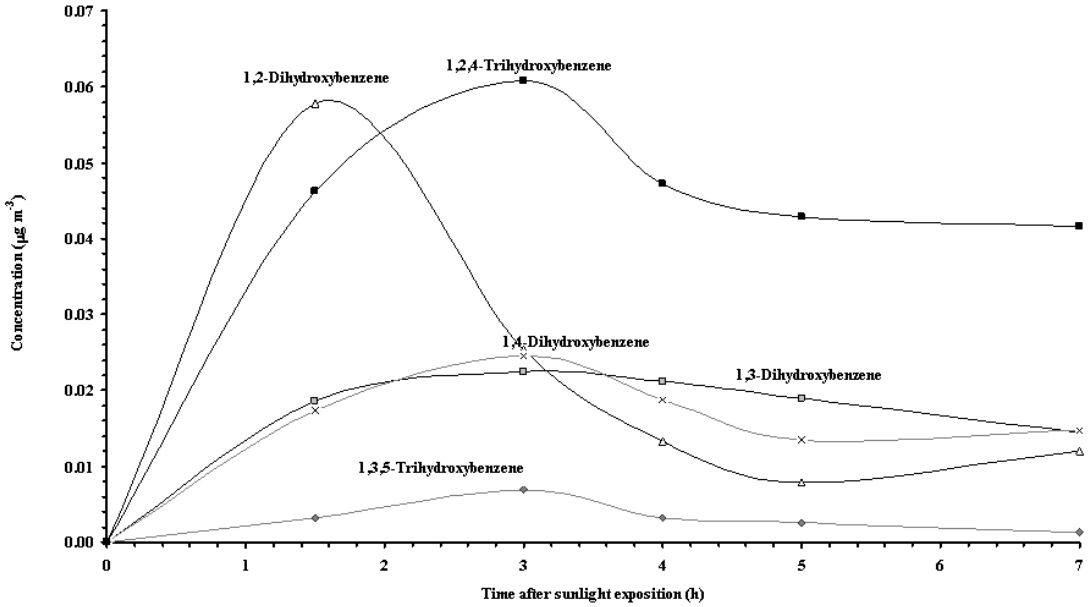

633

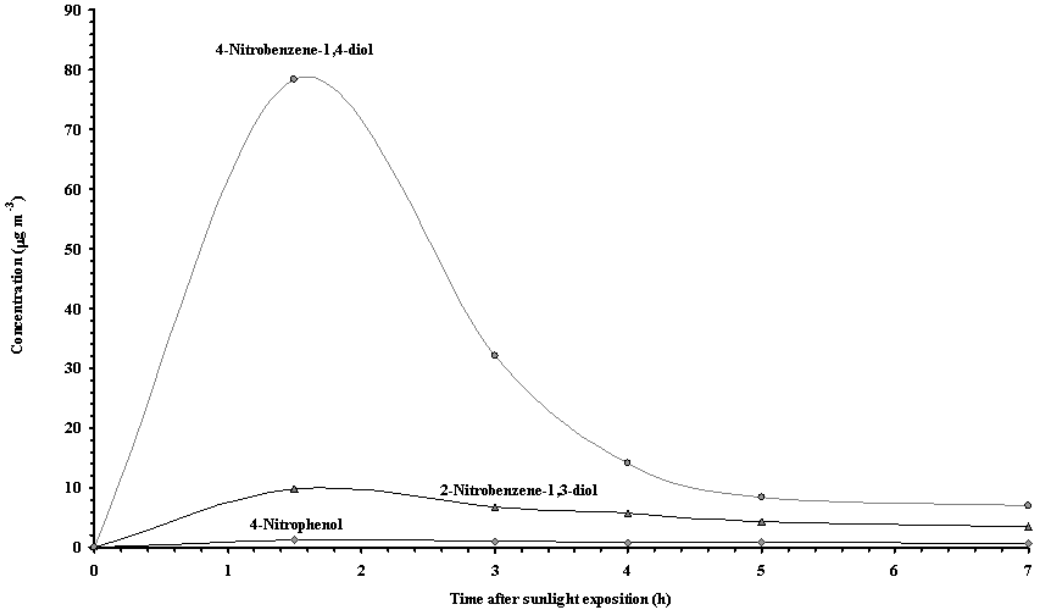

634
635
636
637
638
639
640
641
642

643 Figure 7

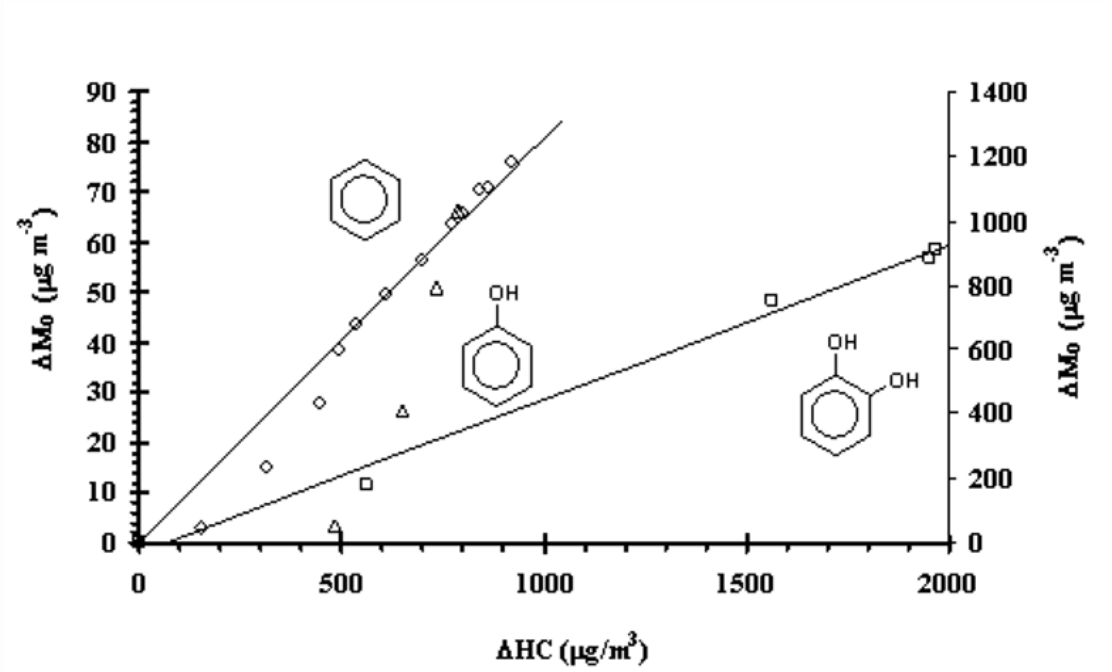

644

645 Figure 8

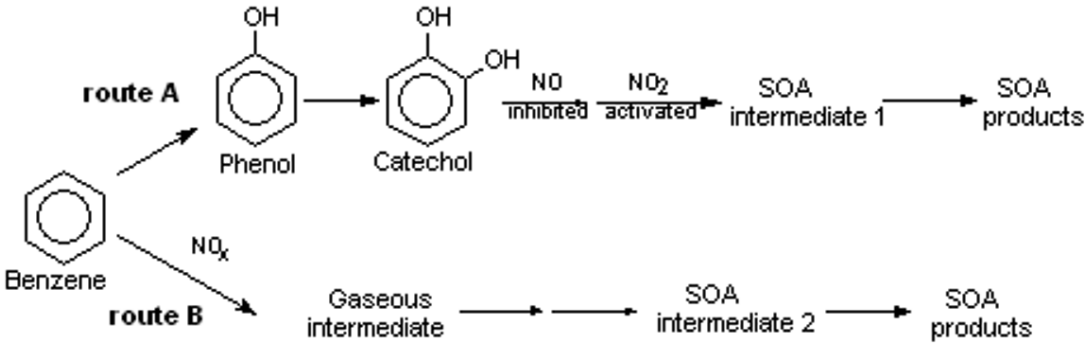

646

647